MOLECULAR AND CELLULAR BIOLOGY, Nov. 2011, p. 4513–4523 Vol. 31, No. 22
0270-7306/11/$12.00 doi:10.1128/MCB.05733-11

The Fbx4 Tumor Suppressor Regulates Cyclin D1 Accumulation and Prevents Neoplastic Transformation▽

Laura Pontano Vaites,[1,2] Eric K. Lee,[1,2] Zhaorui Lian,[1,2] Olena Barbash,[1,2] Darshan Roy,[3] Mariusz Wasik,[3] Andres J. P. Klein-Szanto,[4] Anil K. Rustgi,[5,6,7,8] and J. Alan Diehl[1,2,8]*

The Leonard and Madlyn Abramson Family Cancer Research Institute,[1] Department of Cancer Biology,[2] and Department of Pathology and Laboratory Medicine,[3] University of Pennsylvania, Philadelphia, Pennsylvania 19104; Histopathology Facility, Fox Chase Cancer Center, Philadelphia, Pennsylvania 19111[4]; and Division of Gastroenterology,[5] Department of Medicine,[6] Department of Genetics,[7] and Abramson Cancer Center,[8] University of Pennsylvania, Philadelphia, Pennsylvania 19104

Received 1 June 2011/Returned for modification 24 June 2011/Accepted 26 August 2011

Skp1-Cul1-F-box (SCF) E3 ubiquitin ligase complexes modulate the accumulation of key cell cycle regulatory proteins. Following the G_1/S transition, SCF^{Fbx4} targets cyclin D1 for proteasomal degradation, a critical event necessary for DNA replication fidelity. Deregulated cyclin D1 drives tumorigenesis, and inactivating mutations in Fbx4 have been identified in human cancer, suggesting that Fbx4 may function as a tumor suppressor. $Fbx4^{+/-}$ and $Fbx4^{-/-}$ mice succumb to multiple tumor phenotypes, including lymphomas, histiocytic sarcomas and, less frequently, mammary and hepatocellular carcinomas. Tumors and premalignant tissue from $Fbx4^{+/-}$ and $Fbx4^{-/-}$ mice exhibit elevated cyclin D1, an observation consistent with cyclin D1 as a target of Fbx4. Molecular dissection of the Fbx4 regulatory network in murine embryonic fibroblasts (MEFs) revealed that loss of Fbx4 results in cyclin D1 stabilization and nuclear accumulation throughout cell division. Increased proliferation in early passage primary MEFs is antagonized by DNA damage checkpoint activation, consistent with nuclear cyclin D1-driven genomic instability. Furthermore, $Fbx4^{-/-}$ MEFs exhibited increased susceptibility to Ras-dependent transformation *in vitro*, analogous to tumorigenesis observed in mice. Collectively, these data reveal a requisite role for the SCF^{Fbx4} E3 ubiquitin ligase in regulating cyclin D1 accumulation, consistent with tumor suppressive function *in vivo*.

Cell cycle progression is intricately controlled by coordinated expression and ubiquitin-dependent degradation of key regulatory proteins. Ubiquitylation of target substrates requires the concerted activity of an Ub-activating enzyme (E1), recruitment of an Ub-conjugating enzyme (E2), and an E3 ubiquitin ligase. Although some E3 ubiquitin ligases directly mediate transfer of ubiquitin, for example, the HECT-domain family of E3 ligases, many E3 ligases function as multi-subunit complexes that bridge the charged E2 enzyme with a given substrate (20). The Skp1-Cul1-F-box (SCF) family of E3 ubiquitin ligases is an example of the latter and promotes polyubiquitylation of mainly phosphorylated substrates, including G_1/S regulatory proteins (11, 12, 27, 32, 43). Specificity of SCF ligases is conferred by the F-box protein, which bridges substrate molecules with the core ligase machinery. F-box proteins contain a conserved F-box domain, required for Skp1 binding and recruitment of core ligase components Cul1, Rbx1, and E2, as well as a substrate-recognition domain within the C terminus (39, 43, 51).

The F-box protein, Fbx4, regulates ubiquitylation of cyclin D1, following the G_1/S transition (32). Similar to Fbw7, a ubiquitin ligase for targets such as cyclin E, c-Myc, and Notch (27, 47–50, 54, 55), and β-TrCP, an E3 ligase for targets including IκB, β-catenin, Cdc25A, and Emi1 (10, 16, 18, 24, 26, 28, 36, 38, 45, 46, 52), Fbx4 undergoes dimerization; however, in contrast to either Fbw7 or β-TrCP, Fbx4 dimerization occurs in a cell cycle-dependent manner (5, 17, 44, 46). Fbx4 dimerization requires glycogen synthase kinase 3β (GSK3β)-dependent phosphorylation at serine 12, which triggers ligase activation at the G_1/S transition (5, 32). Critically, mutations that stabilize cyclin D1 and thereby trigger nuclear accumulation of active cyclin D1/CDK4 drive cell transformation (1–3). While cyclin D1 overexpression occurs in multiple human malignancies (4, 6–8, 14, 19, 21–23, 25), overexpression of wild-type cyclin D1 in an Fbx4-proficient system is insufficient to drive spontaneous transformation (3, 5), supporting a model wherein cytoplasmic recognition of phosphorylated cyclin D1 by Fbx4 is sufficient to maintain cellular integrity.

Cyclin D1 mutations that impede degradation and trigger nuclear accumulation promote neoplastic growth (1, 3, 5, 9, 35, 37); however, such mutations are rare in human cancer. Recent work identified inactivating Fbx4 mutations in human cancers that impair ligase phosphorylation and dimerization. Such tumors exhibit marked cyclin D1 nuclear accumulation, highlighting a novel mechanism for cyclin D1 deregulation in cancer (5). Taken together, these findings suggest that Fbx4 is a tumor suppressor, preventing aberrant cyclin D1 accumulation.

To investigate the tumor suppressor function of Fbx4, we ablated the murine *Fbx4* gene. $Fbx4^{-/-}$ mice are viable and lack major developmental defects. However, $Fbx4^{-/-}$ murine embryonic fibroblasts (MEFs) exhibit cyclin D1 stabilization and subsequent nuclear localization, with concomitant induction of DNA damage, consistent with a model wherein nuclear cyclin D1/CDK4 kinase drives genomic instability. Finally,

* Corresponding author. Mailing address: 454 BRB II/III 421 Curie Boulevard, Philadelphia, PA 19104. Phone: (215) 746-6389. Fax: (215) 746-5511. E-mail: adiehl@mail.med.upenn.edu.

▽ Published ahead of print on 12 September 2011.

Fbx4 deficiency facilitates cellular transformation *in vitro*, and both Fbx4$^{+/-}$ and Fbx4$^{-/-}$ mice succumb to multiple tumor phenotypes *in vivo* with a marked increase in cyclin D1 levels, supporting the notion that Fbx4 is a *bona fide* tumor suppressor.

MATERIALS AND METHODS

Targeting vector construction and generation of Fbx4$^{-/-}$ mice. The engineered construct targeting murine *Fbx4* exon 2 was developed by Vega Biolab (Philadelphia, PA). The targeting vector was electroporated into embryonic stem (ES) cells, and clones harboring a correctly targeted allele with a normal karyotype were injected in B6 blastocysts by the University of Pennsylvania core facility for generation of chimeric mice with germ line transmission; these mice were intercrossed with EIIa-Cre transgenic mice to generate Fbx4 heterozygous progeny. The genotypes were verified by PCR using tail DNA. Extraction and PCR were performed with an Extract-N-Amp tissue PCR kit (Sigma-Aldrich). The genotyping primers were as follows: 1loxP forward, 5′-GGCAGAGCTTGAGT TTGCAACATTTCAGGTG-3′, and 3loxP reverse, 5′-TCCTGATCTTTGGAA ATTCTTCCTCTGAGT-3′. Aged mice were monitored closely for signs of distress or palpable tumor mass according to IACUC guidelines, and event-free survival was assessed by Kaplan-Meier analysis.

Southern blot analysis. 5′ and 3′ probes in the genomic region flanking *Fbx4* exons 1 to 3 (site of homologous recombination [see Fig. 1]) were generated. The 5′ probe generates a 15-kb band for the normal *Fbx4* locus and a 10-kb band for an allele that has undergone homologous recombination.

Histology and IHC. Tissues were fixed in 10% buffered formalin overnight, followed by dehydration in a series of ethanol and paraffin embedding and sectioning. Antibodies utilized for immunohistochemistry (IHC) staining were purified cyclin D1 (72-13G; Santa Cruz), Ki-67 (Novocastra), phospho-ATM (Millipore), and γH2AX (Millipore).

MEFs and cell culture. Mouse embryos extracted at day 14 of gestation were maintained on a 3T9 passage protocol, cultured in Dulbecco modified Eagle medium (DMEM) containing 10% fetal bovine serum, 2 mM glutamine, 0.1 mM nonessential amino acids, 55 μM β-mercaptoethanol, and 10 μg of gentamicin/ml. For growth curves, 10^5 cells were plated on 35-mm dishes in duplicate and counted every 24 h by using a hemocytometer. Primary MEFs were immortalized by lentiviral infection with p19^{Arf} shRNA vector. Immortalized cells and NIH 3T3 fibroblasts were cultured in complete DMEM containing 10% fetal bovine serum, glutamine, and 1% penicillin-streptomycin. Cell synchronization was achieved by serum starvation for 24 to 48 h, followed by serum stimulation to allow cell cycle entry.

Western analysis and immunoprecipitation. Whole tissues and cultured cells were lysed in Tween 20 buffer containing 50 mM HEPES (pH 8.0), 150 mM NaCl, 2.5 mM EGTA, 1 mM EDTA, 0.1% Tween 20, and protease/phosphatase inhibitors (1 mM phenylmethylsulfonyl fluoride, 20 U of aprotinin/ml, 5 mg of leupeptin/ml, 1 mM dithiothreitol [DTT], 0.4 mM NaF, and 10 mM β-glycerophosphate). Whole tissues were homogenized in Tween 20 buffer with inhibitors, and lysates were sonicated prior to clearing by centrifugation at 4°C for 30 min. Lysate protein concentration was determined by BCA assay, and proteins were resolved by SDS-PAGE, transferred to nitrocellulose membranes, and subjected to immunoblotting. Antibodies utilized include Fbx4 rabbit polyclonal antibodies (YenZym; Rockland Immunochemicals), cyclin D1 mouse monoclonal D1-72-13G, H4R3 (Abcam), γH2AX (Cell Signaling), p53 mouse monoclonal pab421, p21 and cyclin A (Santa Cruz), phosphorylated threonine 286 cyclin D1 antibody (pT286 Cyc D1) and phosphorylated serine 12 Fbx4 antibody (pS12 Fbx4; Yenzym), p19^{Arf} (Abcam), p16^{Ink4a} (Santa Cruz), Cul4a (Bethyl), Cdt1 (Santa Cruz), Chk2 (BD Biosciences), total and cleaved caspase 3 (Cell Signaling), and β-actin (Sigma). For cyclin D1 immune precipitation experiments, cells were lysed in Tween 20 buffer, and 1 mg of total protein was immunoprecipitated with cyclin D1 72-13G antisera for 1 h at 4°C.

Immunofluorescence. Primary MEFs were plated at optimal densities on glass coverslips. For cyclin D1 localization, passage 3 primary MEFs were grown to 70 to 80% density and then fixed in 1:1 methanol-acetone for 10 min at −20°C. Coverslips were dried then rehydrated with phosphate-buffered saline (PBS), blocked with 10% fetal calf serum in PBS, and then incubated with cyclin D1 primary antibody for 1 h. Coverslips were washed with PBS, followed by incubation with anti-mouse Alexa Fluor 546-conjugated secondary antibody for 30 min. Coverslips were washed with PBS, dried by 70 and 100% ethanol washes, and mounted with Vectashield containing DAPI (4′,6′-diamidino-2-phenylindole; Vector Laboratories). For γH2AX focus visualization, passage 3 cells maintained under atmospheric (21%) oxygen conditions or physiological (3%) oxygen tension were plated on glass coverslips at a density of 10^5 cells/well of a six-well plate and cultured for 24 h. The cells were fixed and blocked as described above, followed by incubation with γH2AX antibodies for 2 h. Coverslips were washed with PBS and then incubated with anti-rabbit Alexa Fluor 488-conjugated secondary antibody for 30 min. Coverslips were mounted as described above and visualized with a Nikon Eclipse 80i fluorescence microscope.

***In vivo* ubiquitylation.** Immortalized MEFs were synchronized by serum starvation and stimulated for 15 h to enter early S phase. Cells were treated for 3 h with 10 μM MG132 (Calbiochem) for proteasome inhibition and harvested in Tween 20 buffer containing proteasome and phosphatase inhibitors, 1 mM DTT, 10 mM *N*-ethylmaleimide (NEM), and 20 μM MG132, followed by immune precipitation with cyclin D1 72-13G antibody as described above. Immunoprecipitation samples were resolved by SDS-PAGE on 10% polyacrylamide gels and immunoblotted with phospho-cyclin D1 T286 antibodies and total ubiquitin antibodies to visualize ubiquitylated cyclin D1 laddering.

***In vitro* ubiquitylation.** NIH 3T3 cells were synchronized by serum starvation, followed by serum stimulation to enter S phase. Cells were either untreated or subjected to 10 Gy of gamma irradiation, followed by 30 min of recovery. Cells were then harvested in Tween 20 buffer, and 1 mg of total protein was immunoprecipitated with Fbx4-specific antibody and protein A-Sepharose beads for 4 h at 4°C. Fbx4-containing endogenous SCF complexes were washed four times with Tween 20 buffer and then three times with kinase buffer (20 mM Tris, 40 mM $MgCl_2$, 2.5 mM EGTA). Beads containing SCF^{Fbx4} complexes were then mixed with Sf9-produced purified cyclin D1 substrate, ATP, ubiquitin, E1, E2, MG132, ubiquitin aldehyde, okadaic acid, energy regeneration buffer (20×: 10 mM ATP, 20 mM HEPES [pH 7.4], 10 mM magnesium acetate, 300 mM creatine phosphate, 0.5 mg of creatine phosphokinase/ml), and kinase buffer to a final volume of 50 μl. Reactions were carried out at 37°C for 30 min, followed by SDS-PAGE for visualization of ubiquitylated cyclin D1 by Western blot.

Metaphase spreads. Immortalized MEFs were synchronized by serum starvation, followed by serum stimulation to allow progression into S phase. Cells in mid-S phase were pulsed with hydroxyurea (HU) for 2 h, followed by HU washout and incubation in complete DMEM. Cells were arrested in metaphase by treatment with colcemid for 2 h, harvested, treated with hypotonic KCl solution, and fixed with methanol-acetic acid. Metaphase spreads were dropped onto glass slides and permitted to dry, followed by Giemsa staining (Sigma). The average number of chromatid breaks per cell was scored in two independent biological replicate cell lines for each genotype. For normal lymphocyte or lymphoma cell metaphase spreads, single cell suspensions of splenic or mesenteric node B cells were prepared, and pulsed with HU for 2 h to induce replication stress, followed by HU washout and incubation with colcemid for 2 h to arrest cells in metaphase. Metaphase spreads were dropped and analyzed as described for the MEF cells above.

***In vitro* transformation assays.** Primary passage 3 MEFs were transduced with pBabe-Puro (empty vector) or pBabe-RasV12 retrovirus. At 24 h postinfection, the cells were trypsinized and replated at a density of 1.5×10^5 cells/35 mm plate in duplicate. Cells were cultured in DMEM containing 5% serum, with medium changed every 2 days for 21 days, followed by Giemsa stain to visualize the foci. To assess cyclin D1 dependence, primary passage 4 MEFs were transfected with pBabe-Puro empty vector, pBabe-RasV12, kinase-deficient pSRα-CDK4K35M, or dominant-negative pBabe-cyclin D1T156A. At 24 h posttransfection, the cells were treated with trypsin and plated as described above. In addition, early-passage spontaneously immortalized cells were transfected with the aforementioned constructs, and plated and grown as described above. For spontaneous transformation of p19shRNA-immortalized MEFs, cells were plated at a density of 1.5×10^5/35-mm plate and cultured as described above.

Statistical analysis. Prism GraphPad Software was utilized for generating Kaplan-Meier mouse event-free survival plots and statistical analysis of survival and tumor onset. All other statistical analyses utilized a two-tailed Student *t* test, with *P* values of <0.05 indicating statistical significance. Error bars represent the means ± the standard deviations.

RESULTS

Generation of Fbx4$^{+/-}$ and Fbx4$^{-/-}$ mice. To directly assess the tumor suppressor function of Fbx4, we generated a targeting vector to facilitate deletion of murine *Fbx4* by homologous recombination in ES cells. LoxP sites were inserted flanking exon 2, with a downstream neomycin (Neo) cassette flanked by a third LoxP site. Cre-mediated recombination and deletion of exon 2 removes F-box sequences critical for Skp1 recruitment

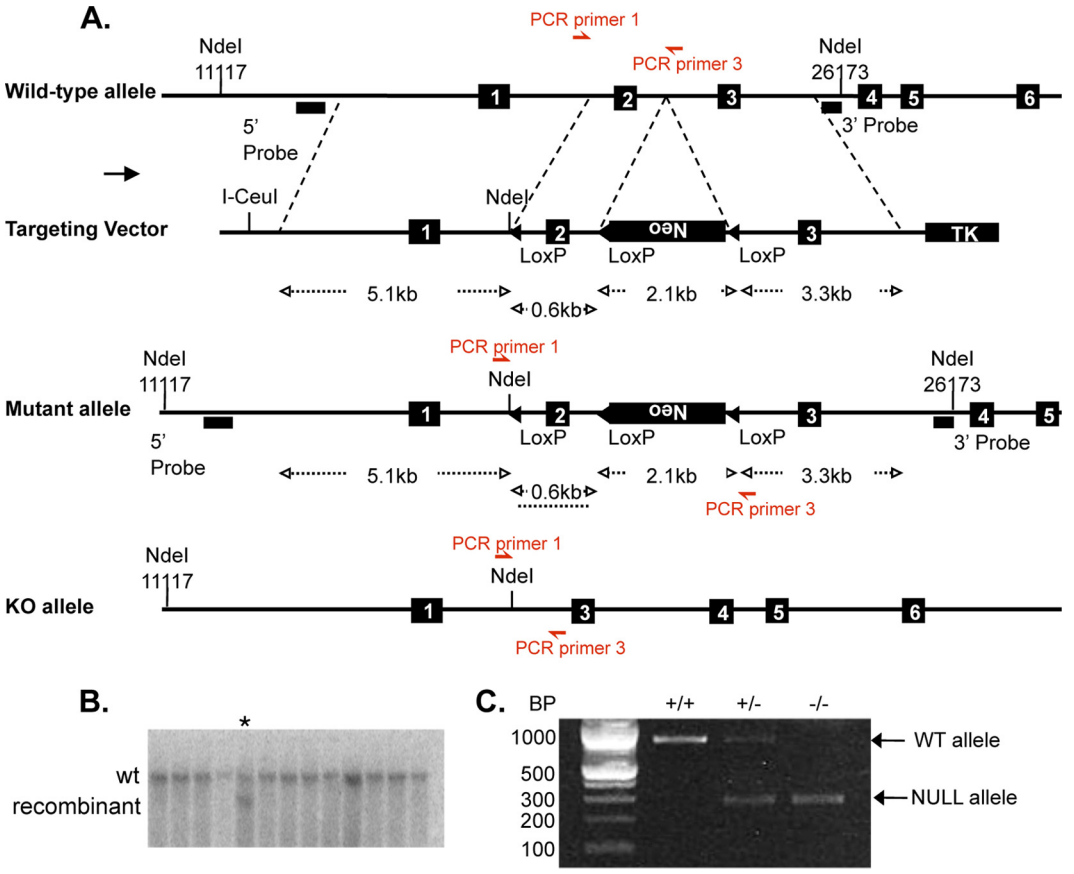

FIG. 1. Generation of Fbx4$^{+/-}$ and Fbx4$^{-/-}$ mice. (A) Vector for targeted disruption of the mouse *Fbx4* locus. Exon 2, encoding the F-box, is flanked by LoxP sites with a downstream neomycin (NEO) resistance cassette flanked by a third LoxP site. (B) Southern blot of a targeted ES clone (denoted by an asterisk) using 5′ probe shown in panel A. (C) Genotyping of Fbx4$^{+/+}$, Fbx4$^{+/-}$, and Fbx4$^{-/-}$ d14 embryos from a heterozygous cross using the tail DNA and PCR primers denoted in panel A.

and assembly of a functional ligase, resulting in a frameshift and premature termination (Fig. 1A). The targeting construct was electroporated into ES cells, and correctly targeted clones were identified by Southern hybridization (Fig. 1B). These clones with a normal karyotype were injected in C57BL/6 blastocysts; two clones resulted in germ line transmission. Chimeric mice were intercrossed with EIIa-Cre transgenic mice to generate Fbx4 heterozygous progeny (genotype confirmation, Fig. 1C). Both Fbx4$^{+/-}$ and Fbx4$^{-/-}$ animals were viable and fertile, with no apparent developmental defects.

Multiple tissues harvested from young (1- to 2-month-old) animals were assessed for cyclin D1 and Fbx4 expression. Importantly, no Fbx4 protein could be detected from the knockout allele using both N- and C-terminal Fbx4-specific antibodies (data not shown), suggesting that deletion of exon 2 creates an inherently unstable protein that is rapidly degraded. Among the tissues examined, cyclin D1 protein accumulation was noted in the mammary gland, lung, thymus, and spleen (Fig. 2A to D). Increased cyclin D1 accumulation was also observed in both Fbx4$^{+/-}$ and Fbx4$^{-/-}$ primary MEFs (Fig. 2E). Reverse transcription-PCR (RT-PCR) analysis revealed equivalent levels of cyclin D1 mRNA in Fbx4$^{+/+}$, Fbx4$^{+/-}$, and Fbx4$^{-/-}$ MEFs, suggesting that protein accumulation occurs at the posttranslational level (Fig. 2F).

Fbx4 deletion promotes cyclin D1 stabilization and nuclear accumulation. To dissect the molecular mechanism underlying cyclin D1 accumulation in Fbx4$^{+/-}$ and Fbx4$^{-/-}$ mice, we prepared MEFs from day 14 (d14) embryos and examined cell proliferation and cyclin D1 stability. Primary Fbx4$^{+/-}$ and Fbx4$^{-/-}$ MEFs exhibited cyclin D1 stabilization in S phase, with increased cyclin D1 half-life (Fig. 3A). Importantly, cyclin D1 stabilization correlated with its robust nuclear accumulation at the expense of cytoplasmic staining in primary MEFs (Fig. 3B). Consistent with cyclin D1 deregulation in the absence of Fbx4, early-passage primary MEFs also exhibited an increased rate of proliferation compared to wild-type MEFs (Fig. 3C). Subsequently, we determined whether cyclin D1 protein is stabilized throughout S phase in Fbx4$^{-/-}$ cells. MEFs were immortalized with p19^{Arf} shRNA, allowing extended culture and effective synchronization, and cyclin D1 levels were assessed across the late-G_1 phase through the mid-S phase. In Fbx4$^{+/+}$ cells, cyclin D1 was rapidly degraded following the G_1/S transition; conversely, cyclin D1 protein was elevated, reflecting increased stability, in Fbx4$^{-/-}$ cells (Fig. 3D). Furthermore, threonine 286 phosphorylated (pT286) cyclin D1 accumulated in Fbx4$^{-/-}$ cells, which is consistent with reduced degradation (Fig. 3E). We also determined whether cyclin D1 S-phase ubiquitylation requires Fbx4. Wild-type and

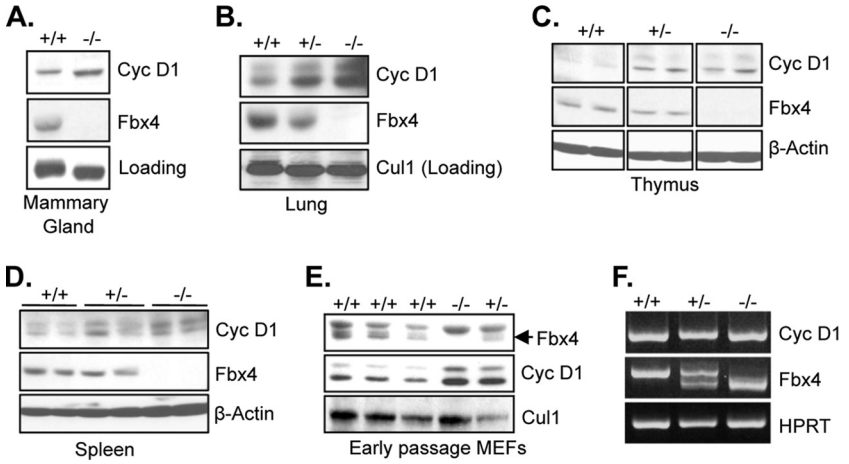

FIG. 2. Cyclin D1 accumulation in $Fbx4^{+/-}$ and $Fbx4^{-/-}$ tissues and MEFs. Tissues were harvested from 1- to 2-month-old mice of each genotype, and lysates were prepared for SDS-PAGE and immunoblotted as indicated. Cyclin D1 accumulation was assessed in mammary glands (A), lungs (B), thymus (C), spleen (D), and primary MEFs (E). (F) Cyclin D1 mRNA is equivalent in $Fbx4^{+/+}$, $Fbx4^{+/-}$, and $Fbx4^{-/-}$ MEFs. RT-PCR was performed on total RNA isolated from MEFs of the indicated genotype using PCR primers specific for cyclin D1 and the housekeeping gene HPRT as a control.

null cells were synchronized and stimulated to enter S phase with serum-derived growth factors; cells were treated with the proteasome inhibitor MG132 to allow accumulation of polyubiquitylated proteins, and cyclin D1 was immunopurified. Immunoblot analysis revealed reduced cyclin D1 polyubiquitylation in $Fbx4^{-/-}$ cells compared to $Fbx4^{+/+}$ controls, suggesting that impaired cyclin D1 ubiquitylation/degradation drives nuclear cyclin D1 accumulation in $Fbx4^{-/-}$ cells (Fig. 3F).

Enhanced proliferation is antagonized by DNA damage in $Fbx4^{-/-}$ MEFs. MEFs were maintained on a 3T9 passage protocol to evaluate the onset of cellular senescence. While early passage $Fbx4^{-/-}$ MEFs initially accumulated to a higher density, proliferation is dramatically reduced between passages 6 and 7 compared to the gradual proliferative decline observed in $Fbx4^{+/+}$ MEFs (Fig. 4A). Both wild-type and null MEFs exhibited similar patterns of senescence-associated $p19^{Arf}$ and $p16^{Ink4a}$ induction (Fig. 4B), suggesting that reduced proliferation is not a result of premature senescence. Furthermore, knockdown of $p19^{Arf}$ bypassed cellular senescence, allowing immortalization of $Fbx4^{+/+}$ and $Fbx4^{-/-}$ MEFs; such immortalized cells did not exhibit proliferative defects (Fig. 4C). Given the reduced proliferation observed in passage 6 and 7 $Fbx4^{-/-}$ MEFs, it is important to note that these cells were not actively undergoing apoptosis, since caspase 3 cleavage was minimal in both $Fbx4^{+/+}$ and $Fbx4^{-/-}$ MEFs (Fig. 4D). Significantly, $Fbx4^{-/-}$ MEFs accumulated p53 and $p21^{Cip1}$, as well as γH2AX, a finding consistent with induction of the DNA damage checkpoint in later passages (Fig. 4E). $Fbx4^{-/-}$ cells also accumulated DSB-associated nuclear foci (Fig. 4F), further supporting this notion. Previous studies established that primary MEF proliferation under atmospheric oxygen is limited by oxidative DNA damage, despite maintenance of long telomeres (40). Importantly, while $Fbx4^{-/-}$ MEFs displayed markers of DNA damage earlier than $Fbx4^{+/+}$ counterparts, the DNA damage in $Fbx4^{-/-}$ MEFs could not be rescued by culture under physiological oxygen (3% O_2) (Fig. 4F). Next, we assessed whether immortalized $Fbx4^{+/+}$ and $Fbx4^{-/-}$ cells are sensitive to S-phase DNA damage. $Fbx4^{+/+}$ and $Fbx4^{-/-}$ cells were synchronized in S phase, pulsed with 2 mM HU for 2 h, followed by HU washout and treatment with colcemid to arrest cells in metaphase. Metaphase spreads prepared from $Fbx4^{-/-}$ cells exhibited a significant increase in chromosome alterations compared to wild-type controls (Fig. 4G). Collectively, these data reveal that loss of Fbx4 triggers nuclear cyclin D1 accumulation, DNA damage checkpoint activation, and ultimately genomic instability.

Previous work established that nuclear cyclin D1 promotes DNA rereplication during S phase and continued DNA replication in the presence of S-phase DNA damage, thereby facilitating genomic instability; these phenotypes are driven by nuclear cyclin D1/CDK4-mediated *CUL4* repression and Cdt1 stabilization (1, 41). Consistent with these findings, Cdt1 protein was stabilized throughout S phase in $Fbx4^{-/-}$ cells, with a concomitant reduction in Cul4A expression (Fig. 5A). Our data revealed attenuated cyclin D1 turnover in primary S-phase $Fbx4^{-/-}$ MEFs (Fig. 3A); furthermore, cyclin D1 degradation in response to S-phase DNA damage was impaired in $Fbx4^{-/-}$ MEFs (Fig. 5B), suggesting that Fbx4 mediates cyclin D1 destruction during unperturbed S-phase progression and following S-phase DNA damage. Since GSK3β phosphorylates Fbx4, triggering ligase dimerization and activation (5), and GSK3β activity increases following S-phase DNA damage (30, 41), we next ascertained whether Fbx4 phosphorylation and ligase activity are regulated by S-phase DNA damage. Treatment of S-phase cells with ionizing radiation enhanced Fbx4 phosphorylation, concomitant with elevated cyclin D1 phosphorylation (Fig. 5C). Moreover, SCF^{Fbx4} E3 ubiquitin ligase activity toward cyclin D1 substrate *in vitro* was markedly increased when SCF^{Fbx4} complexes were purified from S-phase NIH 3T3 cells subjected to ionizing radiation (Fig. 5D). Together, these data indicate that both phosphorylation-dependent cyclin D1 nuclear export and phosphorylation-dependent Fbx4 ligase activation synergize to promote cyclin D1 ubiqui-

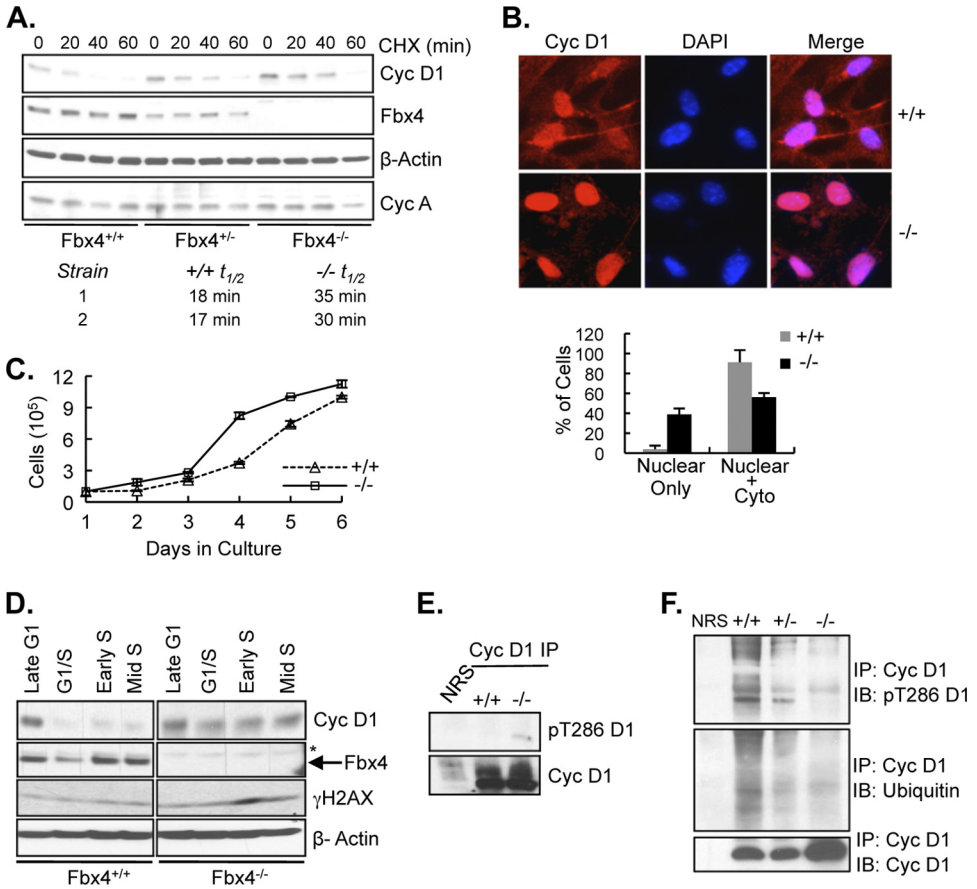

FIG. 3. Fbx4 loss promotes cyclin D1 stabilization and nuclear accumulation in MEFs. (A) Cyclin D1 $t_{1/2}$ is extended in S-phase Fbx4$^{-/-}$ MEFs. In the top panel, synchronous S-phase MEFs were treated with cycloheximide (CHX) as indicated; cell lysates were subjected to SDS-PAGE and immunoblotted for cyclin D1, Fbx4, and cyclin A as an S-phase marker. The bottom panel shows the calculated cyclin D1 $t_{1/2}$ for two independent replicates per genotype. (B) Nuclear cyclin D1 accumulation in Fbx4$^{-/-}$ MEFs. In the top panel, passage 3 MEFs were stained with cyclin D1-specific antibodies and DAPI. Images were captured at ×20 magnification, with equal exposure. The bottom panel shows quantification of nuclear cyclin D1 staining. (C) Fbx4$^{-/-}$ MEFs exhibit increased proliferation. A total of 10^5 Fbx4$^{+/+}$ and Fbx4$^{-/-}$ MEFs (passage 2) were plated in duplicate on 35-mm plates and counted daily. (D) Elevated cyclin D1 protein in S-phase Fbx4$^{-/-}$ cells. p19shRNA-immortalized cells were synchronized by serum starvation, and lysates were immunoblotted as indicated; the asterisk indicates a nonspecific band. (E) Phosphorylated cyclin D1 accumulates in S-phase Fbx4$^{-/-}$ cells. Total cyclin D1 was immunoprecipitated from S-phase cell lysates and immunoblotted for phospho-T286 cyclin D1 (pT286 D1) and total cyclin D1. (F) Cyclin D1 ubiquitylation following the G_1/S transition is impaired in Fbx4$^{-/-}$ cells. The cells were synchronized by serum starvation and stimulated to enter early S phase. Total cyclin D1 was immunoprecipitated from cell lysates, subjected to SDS-PAGE, and immunoblotted to visualize cyclin D1 laddering. Panels: top, a pT286 cyclin D1 immunoblot; middle, total ubiquitin immunoblot; bottom, total cyclin D1 immunoblot.

tylation following S-phase DNA damage, thereby preserving genome integrity.

Fbx4 loss cooperates with RasV12 *in vitro*. The data provided demonstrate that cyclin D1 is deregulated, leading to its nuclear accumulation in the absence of Fbx4. Because cyclin D1 overexpression cooperates with Ras to induce cellular transformation (34), we considered whether Fbx4$^{+/-}$ or Fbx4$^{-/-}$ primary MEFs were susceptible to transformation induced by expression of only oncogenic Ha-RasV12. Infection of early passage MEFs with retroviruses harboring empty vector or oncogenic RasV12 resulted in focus formation in both Fbx4$^{+/-}$ and Fbx4$^{-/-}$ MEFs but not in Fbx4$^{+/+}$ MEFs (Fig. 6A). Although overexpression of wild-type cyclin D1 alone does not promote cell transformation or tumorigenesis in immunocompromised mice (42), expression of cyclin D1 mutants that are stably retained in the nucleus is oncogenic (3). Critically, Ras-driven transformation in Fbx4$^{-/-}$ primary MEFs was dependent upon cyclin D1/CDK4 activity, since the expression of kinase-defective CDK4K35M or dominant-negative cyclin D1T156A suppressed the transforming phenotype (Fig. 6B). In addition, expression of cyclin D1T156A in spontaneously immortalized cells also suppressed Ras-driven transformation in the absence of Fbx4 (Fig. 6C). To determine whether Fbx4 loss and subsequent nuclear accumulation of endogenous cyclin D1 permits spontaneous cellular transformation, we examined the capacity of multiple immortalized cell lines of each genotype to form foci *in vitro*. While immortalized Fbx4$^{+/+}$ cells were refractory to spontaneous transformation, Fbx4$^{+/-}$ cells and, to a greater extent, Fbx4$^{-/-}$ cells readily exhibited spontaneous transformation (Fig. 6D), suggesting that Fbx4 plays a requisite role in suppressing cellular transformation *in vitro*.

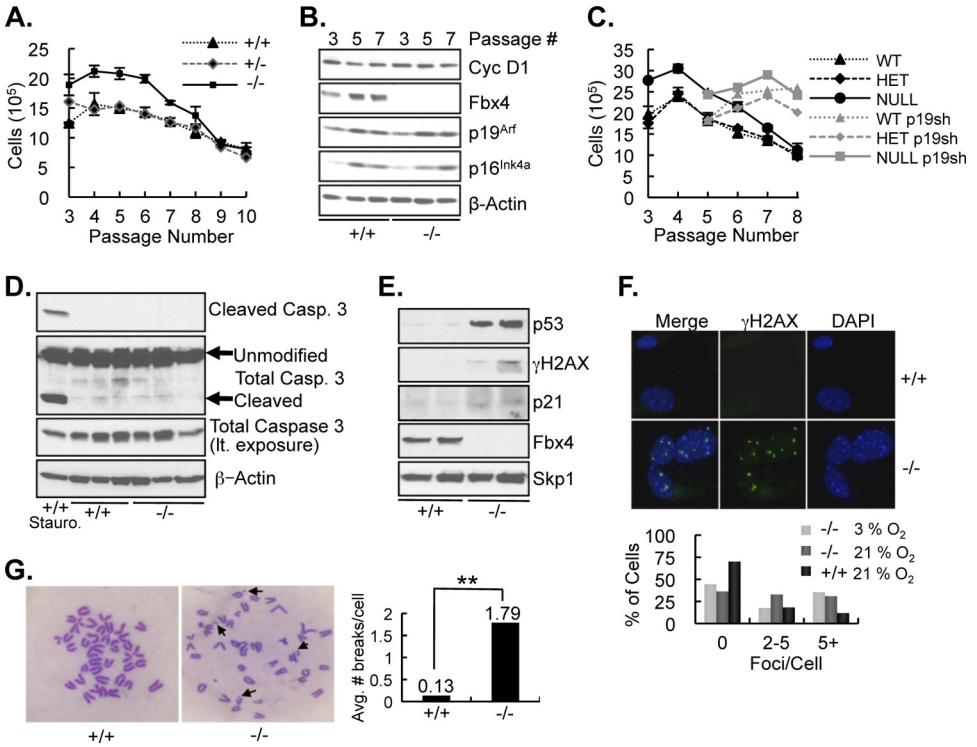

FIG. 4. Enhanced proliferation is antagonized by DNA damage in Fbx4$^{+/-}$ and Fbx4$^{-/-}$ MEFs. (A) MEFs were cultured on a 3T9 passage protocol (9×10^5 cells passaged every 3 days, at least two biological replicates/genotype). The absolute cell count at each passage is displayed. (B) Expression of senescence-associated p19^{Arf} and p16^{Ink4a} in primary MEFs. (C) Knockdown of p19^{Arf} rescues cellular senescence, promoting immortalization. Black curves represent passages of uninfected MEFs; gray curves represent MEFs infected with p19^{Arf} shRNA at passage 4. Immortalized cells proliferate indefinitely beyond passage 8. (D) Minimal caspase 3 cleavage in Fbx4$^{+/+}$ and Fbx4$^{-/-}$ MEFs. Passage 5 MEFs (three independent biological replicates per genotype) were harvested, followed by Western analysis for total and cleaved caspase 3 as a marker for induction of apoptosis. (E) Enhanced p53 and γH2AX induction in Fbx4$^{-/-}$ MEFs. Passage 5 MEF lysates were prepared from two independent isolates/genotype and immunoblotted as indicated. (F) Fbx4$^{-/-}$ MEFs accumulate DNA damage foci. For the top panel, passage 3 MEFs were cultured on coverslips under normoxia (21% O_2) or physiological oxygen tension (3% O_2). The cells were fixed, stained with γH2AX-specific antibodies, and visualized by immunofluorescence. Images were taken at ×60 magnification with equal exposure times. The bottom panel shows a quantification of the percentage of cells exhibiting DNA damage foci. (G) Increased incidence of chromosome alterations in Fbx4$^{-/-}$ MEFs challenged with HU. Two independent immortalized MEF lines per genotype were synchronized by serum starvation, and cells in mid-S-phase were treated with 2 mM HU for 2 h, followed by HU washout and colcemid treatment for 2 h for metaphase arrest. Metaphase spreads were prepared and stained with Giemsa to visualize chromosome alterations. The left panel shows representative images of chromatid breaks; the right panel shows the quantification of the average number of chromatid breaks per cell.

Fbx4$^{+/-}$ and Fbx4$^{-/-}$ mice are tumor-prone. Given the observed cyclin D1 accumulation in normal tissues derived from Fbx4$^{+/-}$ and Fbx4$^{-/-}$ mice and neoplastic transformation phenotype *in vitro*, we investigated whether Fbx4$^{+/-}$ and Fbx4$^{-/-}$ mice develop spontaneous tumors with increasing age. We monitored mice for up to 24 months and observed significant spontaneous tumor formation in both Fbx4$^{+/-}$ and Fbx4$^{-/-}$ mice (Fig. 7A). Fbx4$^{+/-}$ and Fbx4$^{-/-}$ mice exhibited tumors of lymphoblastic lineage, frequent intense myeloid proliferation resulting from severe extramedullary hematopoiesis (EMH), and early myeloid malignancy. These mice developed large cell lymphomas, as confirmed by flow cytometric and immunohistochemical analysis (Table 1). In addition, dendritic cell tumors/histiocytic sarcomas of the spleen, thymus and intestinal wall/mesentery, liver hemangiomas and hepatocellular carcinoma, and tumors of the mammary and uterine epithelium were observed (Table 1).

Fbx4$^{+/-}$ and Fbx4$^{-/-}$ mice succumbed to significant tumor burden with a mean survival of 23 months (Fig. 7A). Importantly, 60.6 and 64.3% of Fbx4$^{+/-}$ and Fbx4$^{-/-}$ mice, respectively, exhibited significant pathology before 24 months of age, highlighting the robust penetrance of these phenotypes. To examine whether tumorigenesis in Fbx4$^{+/-}$ mice was due to haploinsufficiency or loss of heterozygosity, Fbx4 protein expression was analyzed in representative tumor samples. Immunoblot analyses revealed that a majority of Fbx4$^{+/-}$ tumors retained Fbx4 expression, albeit with an approximately 50% reduction in levels compared to the wild type, suggesting that Fbx4 dosage is an important determinant in malignant transformation (Fig. 7B). Consistent with this observation, one wild-type age matched control mouse exhibited severe EMH, a phenotype typically observed in the Fbx4$^{+/-}$ and Fbx4$^{-/-}$ mice; strikingly, immunoblot analysis revealed significant Fbx4 downregulation in this spleen.

Since normal and premalignant Fbx4$^{+/-}$ and Fbx4$^{-/-}$ tissues exhibit cyclin D1 protein accumulation, we ascertained whether cyclin D1 protein expression is elevated in the various tumors. Consistently, elevated cyclin D1 protein was apparent in a majority of lymphomas originating in the mesenteric node of both Fbx4$^{+/-}$ and Fbx4$^{-/-}$ mice, and in livers exhibiting

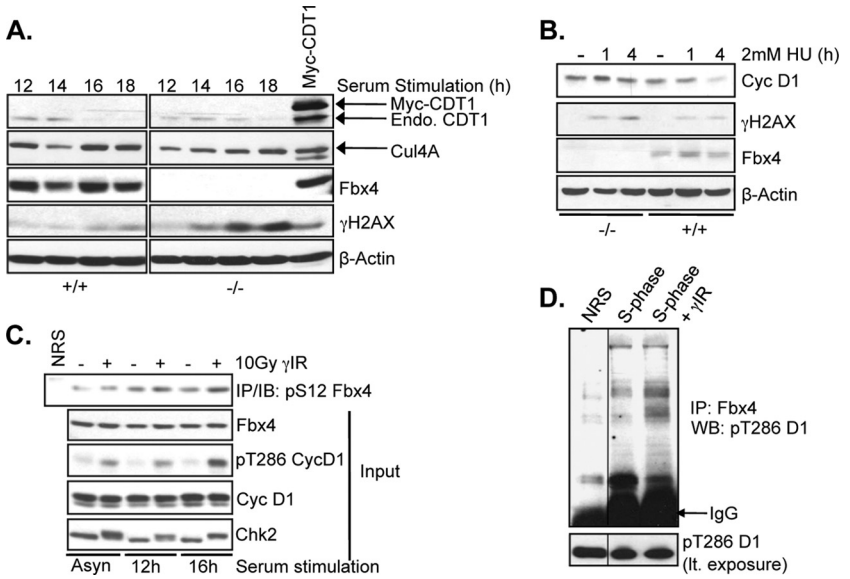

FIG. 5. DNA damage regulates cyclin D1 stability and Fbx4 ligase activation. (A) Stabilization of Cdt1 in immortalized, S-phase-synchronized Fbx4$^{-/-}$ cells. Cells synchronized by serum starvation were serum stimulated for the indicated time (12 h = late G_1; 14, 16, and 18 h = G_1/S, mid-S, and late S phases, respectively), harvested, and subjected to SDS-PAGE and immunoblot analysis for the indicated proteins. (B) S-phase DNA damage-mediated cyclin D1 degradation is attenuated in Fbx4$^{-/-}$ MEFs. Immortalized cells were synchronized by serum starvation, followed by treatment with 2 mM HU; cell lysates were immunoblotted as indicated. (C) Enhanced Fbx4 phosphorylation following S-phase DNA damage. Asynchronous NIH 3T3 cells, or cells synchronized by serum starvation and stimulated (12 h = G_1 phase; 16 h = S phase) were irradiated, followed by recovery for 30 min. The cells were harvested, and lysates were immunoprecipitated with phosphoserine 12 (pS12 Fbx4)-specific antibodies (top panel) to visualize the induction of phosphorylation. The total input lysate immunoblots are shown below. (D) SCF^{Fbx4} ligase activity toward cyclin D1 substrate is enhanced following S-phase DNA damage. SCF^{Fbx4} complexes were immunoprecipitated from S-phase NIH 3T3 cells with or without induction of DNA damage using Fbx4-specific antibodies. Fbx4-containing complexes served as a ligase source for *in vitro* ubiquitylation reactions with Sf9-purified cyclin D1/CDK4 as a substrate, in the presence of E1, E2, ubiquitin, and ATP.

lymphoma infiltrates or hepatocellular carcinoma (Fig. 7C and D). Furthermore, intestinal histiocytic sarcomas and mesenteric node lymphomas exhibited nuclear cyclin D1 accumulation, correlating with increased proliferation, as evidenced by Ki-67 staining (Fig. 7E). Immunoblot and immunohistochemical analyses also revealed a marked induction of γH2AX and phosphorylated ATM, respectively, in lymphoid tumors, which is consistent with nuclear cyclin D1-driven genomic instability (Fig. 7E and F). To further assess sensitivity to genomic instability in wild-type and Fbx4$^{+/-}$ lymphoma cells, we prepared single cell suspensions of primary lymphocytes or lymphoma cells and assessed chromosome alterations following an HU pulse. Loss of Fbx4 significantly increased the incidence of chromatid breaks in lymphoma cells compared to normal lymphoid tissue (Fig. 7G). Finally, DNA sequencing of the p53 DNA-binding domain in lymphoid tumors revealed a premature stop codon insertion and three distinct deletion mutations in the six tumors analyzed (data not shown), suggesting that p53 inactivation may contribute to sustained growth in the presence of DNA damage, thereby facilitating neoplastic transformation. Collectively, these data support a requisite role for Fbx4 in maintaining cell homeostasis *in vitro* and *in vivo* by regulating cyclin D1 accumulation.

DISCUSSION

The SCF^{Fbx4} E3 ubiquitin ligase has been implicated in regulating cyclin D1 turnover in cell culture models; further work revealed a significant role for Fbx4 function in maintaining genomic integrity, highlighted by the relative frequency of mutations that impair its biochemical activity in human tumors. Such mutations occur in a hemizygous manner, consistent with the notion that reduced Fbx4 expression is sufficient for cyclin D1 deregulation and neoplastic transformation (5). Although this evidence suggests that Fbx4 may function as a tumor suppressor, experiments that directly address this question have not been performed. Our analysis demonstrates that Fbx4 loss promotes cyclin D1 overexpression and tumorigenesis, as a significant increase in age-associated malignancy is observed in Fbx4$^{+/-}$ and Fbx4$^{-/-}$ mice compared to wild-type controls. Furthermore, Fbx4 loss in MEFs triggers cyclin D1 stabilization and nuclear localization, and aberrant cyclin D1 regulation in the absence of Fbx4 drives accumulation of DNA damage and subsequent genomic instability, a hallmark of neoplastic transformation. Consistently, the loss of Fbx4 facilitates cell transformation *in vitro*, further emphasizing the tumor suppressive properties of Fbx4.

Fbx4 is a tumor suppressor. Both Fbx4$^{+/-}$ and Fbx4$^{-/-}$ aged mice commonly develop lymphoid malignancies involving the mesenteric lymph node, spleen, liver, and intestine, as well as histiocytic sarcomas/dendritic cell tumors of the spleen, thymus, and intestine, early myeloid malignancies, with mammary, hepatocellular, and uterine carcinomas occurring at lesser frequencies. Fbx4$^{+/-}$ tumors retain Fbx4 expression, which is consistent with human cancer data revealing hemizygous Fbx4 mutations (5). In addition, Fbx4$^{+/-}$ and Fbx4$^{-/-}$ MEFs are susceptible to single-step, Ras-mediated transformation, sup-

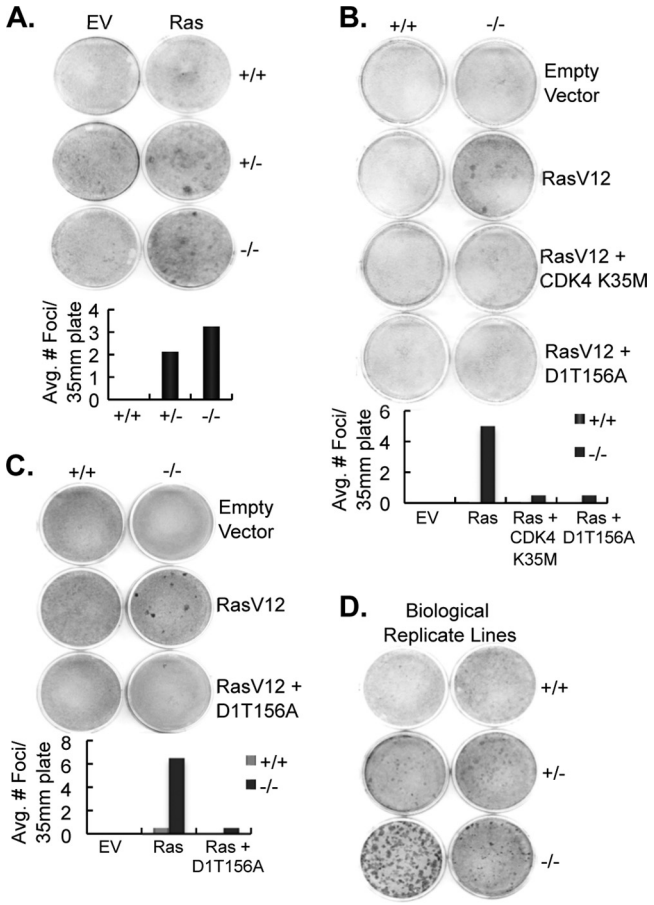

FIG. 6. Fbx4 loss drives cell transformation *in vitro*. (A) Loss of Fbx4 synergizes with oncogenic Ha-RasV12 to promote cell transformation. Primary MEFs (passage 3) were infected with retroviruses harboring empty vector (EV) or RasV12 (Ras) constructs. A total of 1.5×10^5 cells were plated in duplicate on 35-mm plates, grown for 21 days to allow focus formation, and stained with Giemsa to visualize foci. The bottom panel shows the quantification of focus numbers for duplicate plates of each genotype. (B) Primary passage 4 MEFs were transfected with the indicated constructs and plated in duplicate as in panel A to assess focus formation in the presence of kinase-deficient CDK4K35M and dominant-negative cyclin D1T156A. The bottom panel shows the quantification of the focus numbers for duplicate plates. (C) Expression of cyclin D1T156A suppresses RasV12-mediated transformation. Low-passage spontaneously immortalized cells were transfected with the indicated constructs. At 48 h posttransfection, cells were treated with trypsin and plated in duplicate to assess focus formation as in panel A. (D) Spontaneous transformation in immortalized cells. p19shRNA-immortalized cells of each genotype (two independent biological replicate cell lines, passage 15) were plated at a density of 1.5×10^5 cells on 35-mm plates in triplicate and grown as in panel A.

porting the notion that Fbx4 functions as a haploinsufficient tumor suppressor. Importantly, this haploinsufficient function of Fbx4 is not unanticipated, since previous work utilizing RNAi revealed that reduced Fbx4 expression by 60 to 70% is sufficient to promote cyclin D1 stabilization in various epithelial and fibroblast cell lines and anchorage-independent cell growth *in vitro* (5). Although an elevation in cyclin D1 protein in $Fbx4^{+/-}$ and $Fbx4^{-/-}$ epithelial tissue might be expected, the increased cyclin D1 expression in lymphocytes, which typically do not express cyclin D1, and lymphoid tumors were indeed enlightening. These results support a requisite role for posttranslational degradation as a means to limit cyclin D1 accumulation in normal lymphoid tissue, thereby highlighting the tumor-suppressive function of Fbx4 in this tissue. Interestingly, not all tissues exhibiting elevated cyclin D1 develop neoplastic lesions; for example, cyclin D1 is elevated in normal $Fbx4^{+/-}$ and $Fbx4^{-/-}$ lung tissues; however, spontaneous lung adenocarcinomas were not observed. This raises the possibility that the absence of Fbx4 can trigger tissue-specific compensatory pathways for cyclin D1/CDK4 regulation, ultimately antagonizing nuclear function when Fbx4-mediated degradation is impaired.

$Fbx4^{+/-}$ and $Fbx4^{-/-}$ mice develop tumors with a protracted latency that is comparable to pituitary tumors observed in $p18^{Ink4c-/-}$ mice, sarcomas in $p15^{Ink4b-/-}$ mice, and B-cell lymphomas, lung adenocarcinomas, and hepatocellular carcinomas in $U19/EAF2^{-/-}$ mice (29, 53). Although tumors arise in aged mice, it is important to note that this is a remarkably penetrant phenotype, with 38% of $Fbx4^{+/-}$ and $Fbx4^{-/-}$ mice exhibiting substantial lymphoma burden and 23.4% exhibiting EMH before 24 months of age. Furthermore, the frequent incidence of EMH and associated early myeloid malignancy suggests bone marrow failure, and it is of interest to assess the role of Fbx4 in hematopoietic development and bone marrow function in future work.

Loss of Fbx4 promotes cyclin D1 nuclear accumulation and DNA damage. Previous work has linked nuclear cyclin D1 accumulation with tumorigenesis (3, 15, 33). However, the rare incidence of mutations in cyclin D1 that impair its nuclear export and cytoplasmic degradation suggests that other components of the cyclin D1 regulatory machinery, such as Fbx4, are the major targets that confer tumor susceptibility *in vivo*. Consistent with this notion, we observed a substantial extension of cyclin D1 half-life in S-phase $Fbx4^{-/-}$ MEFs, with a significant increase in the rate of proliferation. Importantly, accumulating evidence suggests that cyclin D1 nuclear accumulation during S phase, rather than overt overexpression, underlies its oncogenic function (1, 2, 15, 33).

Consistent with the aforementioned nuclear cyclin D1 phenotype, the initial proliferative advantage observed in $Fbx4^{-/-}$ MEFs dramatically decreases in later passages, suggesting that cells either activate a senescence program prematurely or decrease proliferation as a consequence of DNA damage and/or additional stress responses. Our data support the generation of DNA damage, since DNA damage checkpoint activation is clearly evident in passage 3 to passage 5 MEFs. Importantly, DNA damage observed in $Fbx4^{-/-}$ MEFs is not simply due to oxidative stress, since growth under physiological (3%) O_2 tension does not reduce DNA damage. In addition, DNA damage is not likely to result from stabilization of the other known Fbx4 substrate, Trf1, given that telomere uncapping effects of Trf1 stabilization would take many generations, due to the extremely long telomeres observed in most laboratory mouse lines (31). Nuclear cyclin D1 retention during S phase promotes DNA rereplication and subsequent DNA damage checkpoint activation; mechanistically, nuclear cyclin D1/CDK4 kinase activity is necessary for elevated histone arginine methylation at the *Cul4* promoters, *Cul4* repression, and consequent stabilization of the replication factor Cdt1 (1, 2). In

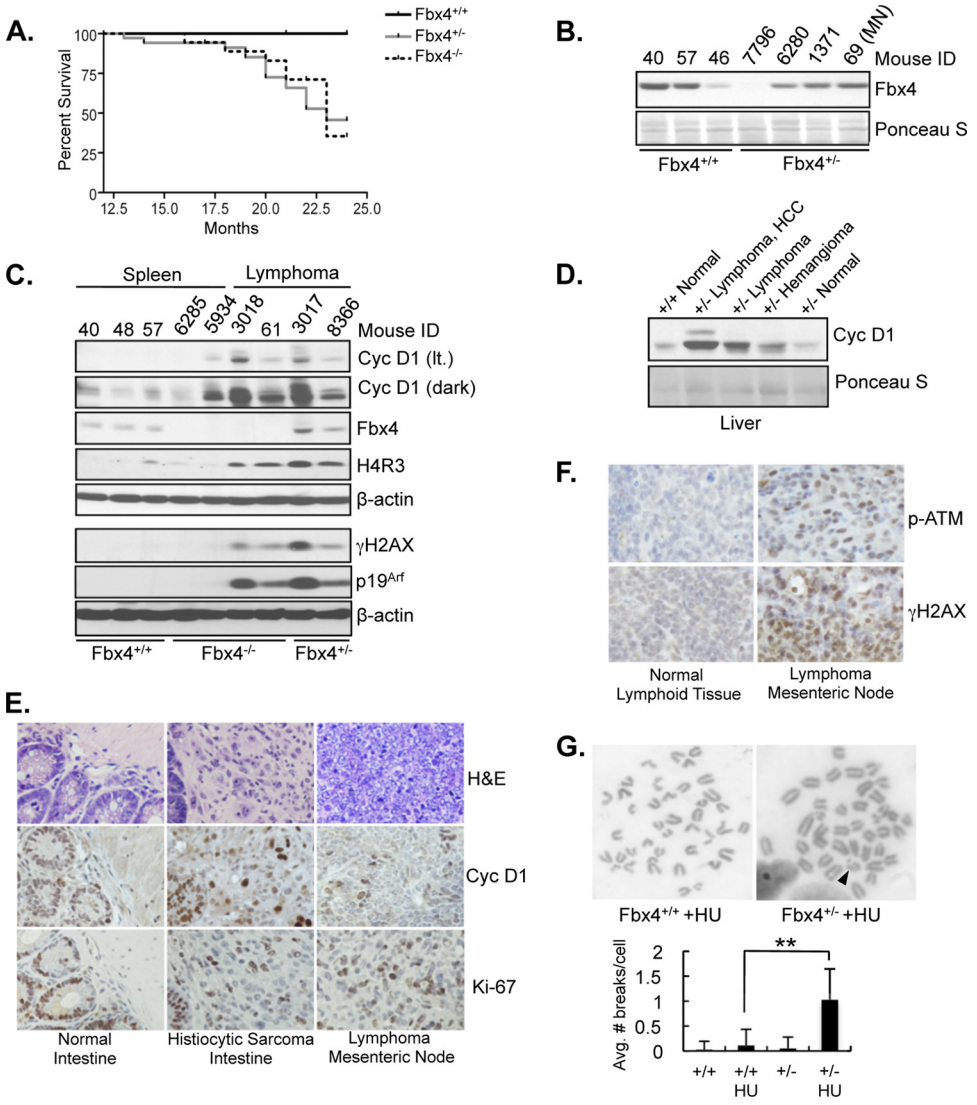

FIG. 7. $Fbx4^{+/-}$ and $Fbx4^{-/-}$ mice are tumor-prone. (A) Kaplan-Meier curves showing the percentage tumor-free survival of $Fbx4^{+/+}$, $Fbx4^{+/-}$, and $Fbx4^{-/-}$ mice to 24 months. (B) Fbx4 haploinsufficiency. Representative tumors arising in $Fbx4^{+/-}$ mice were assessed for Fbx4 protein expression by Western blotting. Only one of four tumors analyzed downregulated Fbx4 expression. (C) $Fbx4^{+/-}$ and $Fbx4^{-/-}$ lymphomas exhibit cyclin D1 accumulation. Lysates prepared from wild-type age-matched spleens, $Fbx4^{-/-}$ spleens, and mesenteric node lymphomas were subjected to SDS-PAGE and immunoblotting as indicated. (D) $Fbx4^{+/-}$ liver tumors exhibit cyclin D1 accumulation. Lysates prepared from $Fbx4^{+/-}$ livers harboring lymphoma, hepatocellular carcinoma (HCC) or hemangioma and normal age-matched livers were analyzed by immunoblot analysis for cyclin D1 levels. (E) Representative hematoxylin and eosin (H&E) and IHC staining for cyclin D1 and Ki-67 as a marker of proliferation in normal intestinal epithelium, $Fbx4^{+/-}$ histiocytic sarcoma of the intestinal muscle wall, and $Fbx4^{-/-}$ primary lymphoma of the mesenteric node. (F) IHC staining for DNA damage markers phosphorylated ATM and γH2AX in $Fbx4^{-/-}$ lymphoma or age-matched wild-type lymphoid tissue. (G) Increased incidence of chromosome alterations in $Fbx4^{+/-}$ lymphoma cells. Mesenteric node and splenic lymphoma cells or wild-type lymphocytes were pulsed with 2 mM HU for 2 h, followed by HU washout and colcemid treatment for 2 h for metaphase arrest. Metaphase spreads were prepared and stained with Giemsa to visualize chromosome alterations. The top panel shows representative images of chromatid breaks; the bottom panel shows the quantification of the average numbers of chromatid breaks per cell.

fact, tumors arising in $Fbx4^{+/-}$ and $Fbx4^{-/-}$ mice exhibit a dramatic increase in histone 4 arginine 3 symmetric dimethylation (Fig. 7C), and $Fbx4^{-/-}$ MEFs exhibit Cdt1 stabilization in S phase, with a concomitant reduction in Cul4 levels (Fig. 5A), supporting the notion that Cdt1 stabilization downstream of nuclear cyclin D1/CDK4 activity drives DNA damage accumulation.

Our previous and current data reveal a tightly regulated mechanistic program for cyclin D1 control in S phase and following DNA damage. Fbx4 serine 12 phosphorylation, an event preceding ligase dimerization and activation, ensures an increased rate of cyclin D1 ubiquitylation following the G_1/S transition. Intriguingly, both nuclear cyclin D1 threonine 286 and cytoplasmic Fbx4 serine 12 are phosphorylated by GSK3β at this point, highlighting the dual regulatory role posttranslational modifications play in coordinating timely cyclin D1 destruction (5, 13). Therefore, it is not surprising that both cyclin D1 threonine 286 and Fbx4 serine 12 phosphorylation events

TABLE 1. Summary of pathology observed in $Fbx4^{+/-}$ and $Fbx4^{-/-}$ mice[a]

Pathology	No. of mice (n = 47)	Incidence (%)
Lymphoblastic lymphoma (spleen, thymus, mesenteric node, liver, intestine)	18	38.3
Extramedullary hematopoiesis/intense myeloid proliferation (spleen, liver)	11	23.4
Hemangioma/angioinvasive tumor (liver, lung)	3	6.4
Dendritic cell tumor (spleen, thymus)/ histiocytic sarcoma (intestine)	3	6.4
Early myeloid tumor	1	2.1
Mammary carcinoma	1	2.1
Uterine tumor	1	2.1

[a] $Fbx4^{+/-}$ and $Fbx4^{-/-}$ mice included as events in the Kaplan-Meier survival analysis frequently develop large cell lymphoblastic lymphomas involving the mesenteric lymph node, spleen, thymus, Peyer's patches of the intestine, and liver. A large percentage of the mice also exhibit extramedullary hematopoiesis and intense myeloid proliferation in the spleen and, less frequently, liver. This is also associated with early myeloid tumor formation. Less commonly observed malignancies include dendritic cell/histiocytic sarcomas, hemangioma, uterine tumor, and mammary carcinoma. Analysis of several mice independent of the Kaplan-Meier cohort also revealed an additional case of intestinal histiocytic sarcoma and a case of hepatocellular carcinoma.

are induced above basal levels following DNA damage, thereby facilitating increased ubiquitin ligase activity toward cyclin D1. Considering that nuclear cyclin D1 promotes DNA rereplication and checkpoint activation (1) and that impaired cyclin D1 degradation in response to S-phase DNA damage drives genomic instability (41), loss or functional inactivation of Fbx4 provides oncogenic insults necessary for neoplastic transformation.

Collectively, our findings support a model in which Fbx4 expression is essential for cell homeostasis in somatic cells. Fbx4 ablation predisposes mice to multiple tumor phenotypes, with concomitant cyclin D1 deregulation and nuclear accumulation. Furthermore, our data suggest that Fbx4 status is an important determinant of neoplastic potential in cells harboring wild-type cyclin D1 overexpression, functioning as a haploinsufficient tumor suppressor. Identification of novel Fbx4 substrates will elucidate additional signaling pathways contributing to the neoplastic phenotype in $Fbx4^{-/-}$ animals, functioning in concert with cyclin D1, and future development of inducible tissue-specific Fbx4-deficient mice will enable Fbx4 ablation in various adult tissues, mirroring the somatic inactivating mutations observed in human cancers.

ACKNOWLEDGMENTS

We thank Petia Zamfirova, Margarita Romero, and Jesi Kim for technical assistance, Serge Fuchs for critical reading of the manuscript, the AFCRI histology core for assistance with paraffin embedding and sectioning, Oren Gilad and Eric Brown for providing $p19^{Arf}$ shRNA lentivirus, and the NIH P30 Center for Molecular Studies in Digestive and Liver Diseases and its Morphology and Molecular Biology Cores.

This study was supported by grants from the National Institutes of Health (CA133154), a Leukemia and Lymphoma Scholar Award (J.A.D.), and P01-CA098101 (A.K.R. and J.A.D.).

REFERENCES

1. **Aggarwal, P., et al.** 2007. Nuclear accumulation of cyclin D1 during S phase inhibits Cul4-dependent Cdt1 proteolysis and triggers p53-dependent DNA rereplication. Genes Dev. **21:**2908–2922.
2. **Aggarwal, P., et al.** Nuclear cyclin D1/CDK4 kinase regulates CUL4 expression and triggers neoplastic growth via activation of the PRMT5 methyltransferase. Cancer Cell **18:**329–340.
3. **Alt, J. R., J. L. Cleveland, M. Hannink, and J. A. Diehl.** 2000. Phosphorylation-dependent regulation of cyclin D1 nuclear export and cyclin D1-dependent cellular transformation. Genes Dev. **14:**3102–3114.
4. **Bani-Hani, K., et al.** 2000. Prospective study of cyclin D1 overexpression in Barrett's esophagus: association with increased risk of adenocarcinoma. J. Natl. Cancer Inst. **92:**1316–1321.
5. **Barbash, O., et al.** 2008. Mutations in Fbx4 inhibit dimerization of the SCF(Fbx4) ligase and contribute to cyclin D1 overexpression in human cancer. Cancer Cell **14:**68–78.
6. **Bartkova, J., et al.** 1994. Cyclin D1 protein expression and function in human breast cancer. Int. J. Cancer **57:**353–361.
7. **Bartkova, J., et al.** 1995. Abnormal patterns of D-type cyclin expression and G1 regulation in human head and neck cancer. Cancer Res. **55:**949–956.
8. **Bartkova, J., J. Lukas, M. Strauss, and J. Bartek.** 1994. The PRAD-1/cyclin D1 oncogene product accumulates aberrantly in a subset of colorectal carcinomas. Int. J. Cancer **58:**568–573.
9. **Benzeno, S., et al.** 2006. Identification of mutations that disrupt phosphorylation-dependent nuclear export of cyclin D1. Oncogene **25:**6291–6303.
10. **Busino, L., et al.** 2003. Degradation of Cdc25A by beta-TrCP during S phase and in response to DNA damage. Nature **426:**87–91.
11. **Carrano, A. C., E. Eytan, A. Hershko, and M. Pagano.** 1999. SKP2 is required for ubiquitin-mediated degradation of the CDK inhibitor p27. Nat. Cell Biol. **1:**193–199.
12. **Deshaies, R. J.** 1999. SCF and Cullin/Ring H2-based ubiquitin ligases. Annu. Rev. Cell Dev. Biol. **15:**435–467.
13. **Diehl, J. A., M. Cheng, M. F. Roussel, and C. J. Sherr.** 1998. Glycogen synthase kinase-3β regulates cyclin D1 proteolysis and subcellular localization. Genes Dev. **12:**3499–3511.
14. **Gillett, C., et al.** 1994. Amplification and overexpression of cyclin D1 in breast cancer detected by immunohistochemical staining. Cancer Res. **54:** 1812–1817.
15. **Gladden, A. B., W. R. P. Aggarwal, M. A. Wasik, and J. A. Diehl.** 2006. Expression of constitutively nuclear cyclin D1 in murine lymphocytes induces B-cell lymphoma Oncogene **25:**998–1007.
16. **Guardavaccaro, D., et al.** 2003. Control of meiotic and mitotic progression by the F box protein beta-Trcp1 in vivo. Dev. Cell **4:**799–812.
17. **Hao, B., S. Oehlmann, M. E. Sowa, J. W. Harper, and N. P. Pavletich.** 2007. Structure of a Fbw7-Skp1-cyclin E complex: multi-site-phosphorylated substrate recognition by SCF ubiquitin ligases. Mol. Cell **26:**131–143.
18. **Hatakeyama, S., et al.** 1999. Ubiquitin-dependent degradation of IκBα is mediated by a ubiquitin ligase Skp1/Cul 1/F-box protein FWD1. Proc. Natl. Acad. Sci. U. S. A. **96:**3859–3863.
19. **Herman, J. G., et al.** 1995. Inactivation of the CDKN2/p16/MTS1 gene is frequently associated with aberrant DNA methylation in all common human cancers. Cancer Res. **55:**4525–4530.
20. **Hershko, A., and A. Ciechanover.** 1998. The ubiquitin system. Annu. Rev. Biochem. **67:**425–479.
21. **Hibberts, N. A., et al.** 1999. Analysis of cyclin D1 (CCND1) allelic imbalance and overexpression in sporadic human pituitary tumors. Clin. Cancer Res. **5:**2133–2139.
22. **Hosokawa, Y., and A. Arnold.** 1998. Mechanism of cyclin D1 (CCND1, PRAD1) overexpression in human cancer cells: analysis of allele-specific expression. Genes Chromosomes Cancer **22:**66–71.
23. **Hosokawa, Y., T. Joh, Y. Maeda, A. Arnold, and M. Seto.** 1999. Cyclin D1/PRAD1/BCL-1 alternative transcript [B] protein product in B-lymphoid malignancies with t(11;14)(q13;q32) translocation. Int. J. Cancer **81:**616–619.
24. **Jin, J., et al.** 2003. SCFbeta-TRCP links Chk1 signaling to degradation of the Cdc25A protein phosphatase. Genes Dev. **17:**3062–3074.
25. **Jin, M., et al.** 2001. Cyclin D1, p16 and retinoblastoma gene product expression as a predictor for prognosis in non-small cell lung cancer at stages I and II. Lung Cancer **34:**207–218.
26. **Kitagawa, M., et al.** 1999. An F-box protein, FWD1, mediates ubiquitin-dependent proteolysis of beta-catenin. EMBO J. **18:**2401–2410.
27. **Koepp, D. M., et al.** 2001. Phosphorylation-dependent ubiquitination of cyclin E by the SCFFbw7 ubiquitin ligase. Science **294:**173–177.
28. **Latres, E., D. S. Chiaur, and M. Pagano.** 1999. The human F box protein beta-Trcp associates with the Cul1/Skp1 complex and regulates the stability of beta-catenin. Oncogene **18:**849–854.
29. **Latres, E., et al.** 2000. Limited overlapping roles of $p15^{INK4b}$ and $p18^{INK4c}$ cell cycle inhibitors in proliferation and tumorigenesis. EMBO J. **19:**3496–3506.
30. **Lee, J. Y., S. J. Yu, Y. G. Park, J. Kim, and J. Sohn.** 2007. Glycogen synthase kinase 3β phosphorylates $p21^{WAF1/CIP1}$ for proteasomal degradation after UV irradiation. Mol. Cell. Biol. **27:**3187–3198.
31. **Lee, T. H., K. Perrem, J. W. Harper, K. P. Lu, and X. Z. Zhou.** 2006. The F-box protein FBX4 targets PIN2/TRF1 for ubiquitin-mediated degradation and regulates telomere maintenance. J. Biol. Chem. **281:**759–768.
32. **Lin, D. I., et al.** 2006. Phosphorylation-dependent ubiquitination of cyclin D1 by the SCF(FBX4-αB crystallin) complex. Mol. Cell **24:**355–366.

33. **Lin, D. I., et al.** 2007. Disruption of cyclin D1 nuclear export and proteolysis accelerates mammary carcinogenesis. Oncogene **27:**1231–1242.
34. **Lovec, H., A. Sewing, F. C. Lucibello, R. Muller, and T. Moroy.** 1994. Oncogenic activity of cyclin D1 revealed through cooperation with Ha-ras: link between cell cycle control and malignant transformation. Oncogene **9:**323–326.
35. **Lu, F., A. B. Gladden, and J. A. Diehl.** 2003. An alternatively spliced cyclin D1 isoform, cyclin D1b, is a nuclear oncogene. Cancer Res. **63:**7056–7061.
36. **Margottin-Goguet, F., et al.** 2003. Prophase destruction of Emi1 by the SCF(betaTrCP/Slimb) ubiquitin ligase activates the anaphase promoting complex to allow progression beyond prometaphase. Dev. Cell **4:**813–826.
37. **Moreno-Bueno, G., et al.** 2003. Cyclin D1 gene (CCND1) mutations in endometrial cancer. Oncogene **22:**6115–6118.
38. **Nakayama, K., et al.** 2003. Impaired degradation of inhibitory subunit of NF-κB (IκB) and β-catenin as a result of targeted disruption of the β-TrCP1 gene. Proc. Natl. Acad. Sci. U. S. A. **100:**8752–8757.
39. **Nakayama, K. I., and K. Nakayama.** 2005. Regulation of the cell cycle by SCF-type ubiquitin ligases. Semin. Cell Dev. Biol. **16:**323–333.
40. **Parrinello, S., et al.** 2003. Oxygen sensitivity severely limits the replicative life span of murine fibroblasts. Nat. Cell Biol. **5:**741–747.
41. **Pontano, L. L., et al.** 2008. Genotoxic stress-induced cyclin D1 phosphorylation and proteolysis are required for genomic stability. Mol. Cell. Biol. **28:**7245–7258.
42. **Quelle, D. E., et al.** 1993. Overexpression of mouse D-type cyclins accelerates G1 phase in rodent fibroblasts. Genes Dev. **7:**1559–1571.
43. **Skowyra, D., K. L. Craig, M. Tyers, S. J. Elledge, and J. W. Harper.** 1997. F-box proteins are receptors that recruit phosphorylated substrates to the SCF ubiquitin-ligase complex. Cell **91:**209–219.
44. **Suzuki, H., et al.** 2000. Homodimer of two F-box proteins βTrCP1 or βTrCP2 binds to IκBα for signal-dependent ubiquitination. J. Biol. Chem. **275:**2877–2884.
45. **Tan, P., et al.** 1999. Recruitment of a ROC1-CUL1 ubiquitin ligase by Skp1 and HOS to catalyze the ubiquitination of I κBα. Mol. Cell **3:**527–533.
46. **Tang, X., et al.** 2007. Suprafacial orientation of the SCFCdc4 dimer accommodates multiple geometries for substrate ubiquitination. Cell **129:**1165–1176.
47. **Tetzlaff, M. T., et al.** 2004. Defective cardiovascular development and elevated cyclin E and Notch proteins in mice lacking the Fbw7 F-box protein. Proc. Natl. Acad. Sci. U. S. A. **101:**3338–3345.
48. **Tsunematsu, R., et al.** 2004. Mouse Fbw7/Sel-10/Cdc4 is required for notch degradation during vascular development. J. Biol. Chem. **279:**9417–9423.
49. **Welcker, M., et al.** 2004. The Fbw7 tumor suppressor regulates glycogen synthase kinase 3 phosphorylation-dependent c-Myc protein degradation. Proc. Natl. Acad. Sci. U. S. A. **101:**9085–9090.
50. **Welcker, M., et al.** 2003. Multisite phosphorylation by Cdk2 and GSK3 controls cyclin E degradation. Mol. Cell **12:**381–392.
51. **Winston, J. T., D. M. Koepp, C. Zhu, S. J. Elledge, and J. W. Harper.** 1999. A family of mammalian F-box proteins. Curr. Biol. **9:**1180–1182.
52. **Winston, J. T., et al.** 1999. The SCFβ-TRCP-ubiquitin ligase complex associates specifically with phosphorylated destruction motifs in IκBα and β-catenin and stimulates IκBα ubiquitination in vitro. Genes Dev. **13:**270–283.
53. **Xiao, W., et al.** 2008. U19/Eaf2 knockout causes lung adenocarcinoma, B-cell lymphoma, hepatocellular carcinoma, and prostatic intraepithelial neoplasia. Oncogene **27:**1536–1544.
54. **Yada, M., et al.** 2004. Phosphorylation-dependent degradation of c-Myc is mediated by the F-box protein Fbw7. EMBO J. **23:**2116–2125.
55. **Ye, X., et al.** 2004. Recognition of phosphodegron motifs in human cyclin E by the SCF(Fbw7) ubiquitin ligase. J. Biol. Chem. **279:**50110–50119.